came significant only when the delay period was longer than 1 s (Sheth and Shimojo, 2004; Obhi and Goodale, 2005), much longer than the duration of the blank period in the present study (300 ms).

We suggest another clear advantage of using the allocentric memory for memorizing the initial target position. Because participants generally make a saccade during the blank period, it is useless to rely on the retinotopic coordinate for memorizing the initial target position. The brain has to rely on the cranial coordinate, but the resolution in the cranial coordinate depends on the error in evaluating the eye position. In natural situations, the head also moves during the reach. Thus, the initial target position should be decoded in terms of the body, and the errors in estimating the eye and head positions additively blur the memory of the initial target position. Conversely, the background is generally stable in natural situations. Thus, the allocentric coordinate offers a reliable frame of reference that is immune to the movements of the body parts. This explains why the brain relies on the allocentric coordinate for evaluating the initial target position and the motor error.

Optimal size and complexity of a background

The smallest figure (8 mm) in experiment 2, which was as small as the target itself, did not yield any significant cancelling effect, nor did the effect of a single line 80 mm in length in experiment 3 reach a level of significance. However, two lines achieved a level of significance. These results generally suggest that the target should be "surrounded" by salient landmarks at the time of encoding to form an effective background coordinate.

With respect to the size of the center square that surrounded the target (experiment 2), the cancelling effect was optimal when the center square was 40 mm compared with when the center square was 80 or 120 mm. The optimal size can be explained in terms of the minimal distance between the target and the square at the time of encoding. Lemay et al. (2004) reported that the error in a delayed reaching task with a background square became smaller when the target was located closer to the side of the square. In the present study, a target was presented at a random location within a circle (20 mm radius) with its center at the center of the middle square. Thus, the minimal distance ranged from 0 to 20 mm when the size of the square was 40 mm; this was much smaller than the distances with larger squares (20–40 mm at width of 80 mm and 40–60 mm at width of 120 mm). Similar results were reported by Krigolson et al. (2007).

The optimal size of the background can also be explained in terms of the saliency of the change attributable to the shift of the background by 20 mm. As mentioned, the target was presented at a random location within a circle (20 mm radius). Thus, the target was located outside the center square with a probability of 0.5 when the center square was 40 mm in width. In contrast, the target remained within the center square when the square was 80 or 120 mm wide. The "jump" over the vertical side of the square would serve as a strong indication that a target has moved out of the frame. In this case, the brain would have directly depended on the allocentric memory of the initial target position within the square to evaluate the motor error.

Finally, it is worth noting that the cancelling effect with the 80 mm square was much enhanced by adding many smaller squares. Because the distribution of the distance between the target and each side of the square was unchanged, the results indicate that the "mass" of the figures represents another important factor in whether the figures are regarded as a background.

Natural scenes are full of details and salient features that surround a target to be reached. It is thus reasonable to expect that the background coordinate is actually used in our daily lives for evaluating the error of our reaching movements by presenting the initial target position. The remaining question is how the initial target position is represented in terms of the background in the brain. One extreme possibility is that our brain takes a snapshot of the landscape and maps the initial target position on the snapshot. A new snapshot after a blank is overlaid to the old one on the basis of pixelwise similarity, so that a heavy background would dominate over a single target. Another extreme possibility is that the landscape is parsed into a number of independent objects, each of which and the target itself may be represented even in the egocentric coordinate. Then, the initial target position is encoded as a combination of vectors drawn from each object to the target. Assuming that this hypothesis is true, allocentric process could be performed by neurons that encode object positions in egocentric coordinates and that the brain may not distinguish between target and background, per se. Either theory does not contradict with the results at present. Whether and how the "background coordinate" is represented in the brain merits additional investigation.

References

Blohm G, Crawford JD (2007) Computations for geometrically accurate visually guided reaching in 3-D space. J Vis 7:4 1–22. CrossRef Medline

Boi M, Vergeer M, Ogmen H, Herzog MH (2011) Nonretinotopic exogenous attention. Curr Biol 21:1732–1737. CrossRef Medline

Bridgeman B, Klassen H (1983) On the origin of stroboscopic induced motion. Percept Psychophys 34:149–154. CrossRef Medline

Bridgeman B, Peery S, Anand S (1997) Interaction of cognitive and sensorimotor maps of visual space. Percept Psychophys 59:456–469. CrossRef Medline

Burgess N, Spiers HJ, Paleologou E (2004) Orientational manoeuvres in the dark: dissociating allocentric and egocentric influences on spatial memory. Cognition 94:149–166. CrossRef Medline

Byrne PA, Crawford JD (2010) Cue reliability and a landmark stability heuristic determine relative weighting between egocentric and allocentric visual information in memory-guided reach. J Neurophysiol 103:3054–3069. CrossRef Medline

Byrne PA, Cappadocia DC, Crawford JD (2010) Interactions between gaze-centered and allocentric representations of reach target location in the presence of spatial updating. Vision Res 50:2661–2670. CrossRef Medline

Carrozzo M, Stratta F, McIntyre J, Lacquaniti F (2002) Cognitive allocentric representations of visual space shape pointing errors. Exp Brain Res 147:426–436. CrossRef Medline

Chen Y, Byrne P, Crawford JD (2011) Time course of allocentric decay, egocentric decay, and allocentric-to-egocentric conversion in memory-guided reach. Neuropsychologia 49:49–60. CrossRef Medline

Dassonville P, Bala JK (2004) Perception, action, and Roelofs effect: a mere illusion of dissociation. PLoS Biol 2:e364. CrossRef Medline

Dassonville P, Bridgeman B, Kaur Bala J, Thiem P, Sampanes A (2004) The induced Roelofs effect: two visual systems or the shift of a single reference frame? Vision Res 44:603–611. CrossRef Medline

Day BL, Lyon IN (2000) Voluntary modification of automatic arm movements evoked by motion of a visual target. Exp Brain Res 130:159–168. CrossRef Medline

Day RW, Quinn GP (1989) Comparisons of treatments after an analysis of variance in ecology. Ecol Monogr 59:433–463. CrossRef

Henriques DY, Klier EM, Smith MA, Lowy D, Crawford JD (1998) Gaze-centered remapping of remembered visual space in an open-loop pointing task. J Neurosci 18:1583–1594. Medline

Kawato M, Furukawa K, Suzuki R (1987) A hierarchical neural-network model for control and learning of voluntary movement. Biol Cybern 57:169–185. CrossRef Medline

Kitazawa S, Yin PB (2002) Prism adaptation with delayed visual error signals in the monkey. Exp Brain Res 144:258–261. CrossRef Medline

Kitazawa S, Kohno T, Uka T (1995) Effects of delayed visual information on

the rate and amount of prism adaptation in the human. J Neurosci 15: 7644–7652. Medline

Krigolson O, Heath M (2004) Background visual cues and memory-guided reaching. Hum Mov Sci 23:861–877. CrossRef Medline

Krigolson O, Clark N, Heath M, Binsted G (2007) The proximity of visual landmarks impacts reaching performance. Spat Vis 20:317–336. CrossRef Medline

Lemay M, Bertram CP, Stelmach GE (2004) Pointing to an allocentric and egocentric remembered target. Motor Control 8:16–32. Medline

McIntyre J, Stratta F, Lacquaniti F (1997) Viewer-centered frame of reference for pointing to memorized targets in three-dimensional space. J Neurophysiol 78:1601–1618. Medline

McIntyre J, Stratta F, Lacquaniti F (1998) Short-term memory for reaching to visual targets: psychophysical evidence for body-centered reference frames. J Neurosci 18:8423–8435. Medline

Obhi SS, Goodale MA (2005) The effects of landmarks on the performance of delayed and real-time pointing movements. Exp Brain Res 167:335–344. CrossRef Medline

Oldfield RC (1971) The assessment and analysis of handedness: the Edinburgh inventory. Neuropsychologia 9:97–113. CrossRef Medline

Roelofs C (1935) Optische Localisation. Arch Augenheilkunde 109: 395–415.

Sheth BR, Shimojo S (2004) Extrinsic cues suppress the encoding of intrinsic cues. J Cogn Neurosci 16:339–350. CrossRef Medline

Soechting JF, Flanders M (1989) Sensorimotor representations for pointing to targets in three-dimensional space. J Neurophysiol 62: 582–594. Medline

Tanaka H, Sejnowski TJ (2013) Computing reaching dynamics in motor cortex using Cartesian spatial coordinates. J Neurophysiol 109:1182–1201. CrossRef Medline

Vetter P, Goodbody SJ, Wolpert DM (1999) Evidence for an eye-centered spherical representation of the visuomotor map. J Neurophysiol 81:935–939. Medline

IEEJ TRANSACTIONS ON ELECTRICAL AND ELECTRONIC ENGINEERING
IEEJ Trans 2013; **8**: 310–312
Published online in Wiley Online Library (wileyonlinelibrary.com). DOI:10.1002/tee.21860

Letter

Sputtering Condition Optimization of Sputtered IrOx and TiN Stimulus Electrodes for Retinal Prosthesis

Yi-Li Pan, Non-member
Toshihiko Noda, Member
Kiyotaka Sasagawa, Non-member
Takashi Tokuda, Member
Jun Ohta[a], Member

We have optimized the sputtering conditions for sputtered IrOx and TiN electrodes for retinal prosthesis. The basic electrochemical characteristics were evaluated by cyclic voltammetry, and the surface morphology was inspected by atomic force microscopy. To measure the charge delivery capacity (CDC), a 300-μm diameter electrode was formed, a balanced biphasic current pulse was applied, and the voltage response was measured. From the experimental results, the CDCs of IrOx and TiN in the best sputtering conditions were improved by more than 8 and 4 times compared to that of Pt, respectively. © 2013 Institute of Electrical Engineers of Japan. Published by John Wiley & Sons, Inc.

Keywords: IrOx, TiN, stimulus electrode, retinal prosthesis

Received 02 September 2012; Revised 03 October 2012

1. Introduction

Retinal prosthesis is considered as a good means to treat those who have lost their sight due to degenerative retinal diseases[1]. A retinal prosthesis is implanted into the eye to replace the damaged photoreceptor cells, and a patterned electrical stimulation pulse through the retinal prosthesis can stimulate the remaining neural cells to partially restore sight.

The electrode plays an important link between the electronic device and human tissue. The number of electrodes determines the resolution of the electrically elicited image by retinal prosthesis. Pt is the most often used electrode material in neural stimulation devices; however, it has been pointed out that its charge delivery capacity (CDC) is not enough. Therefore, high CDC materials such as IrOx and TiN are desired to form smaller electrodes to increase the number of electrodes in the limited area.

In this letter, we report the optimization of the sputtering conditions for IrOx and TiN sputtering deposition. The characteristics of the sputtered IrOx and TiN were evaluated by cyclic voltammetry (CV) and the voltage response of the inputted biphasic current pulse. In addition, the surface morphology was inspected by atomic force microscopy (AFM).

2. Experimental Methods

IrOx and TiN thin films were fabricated by sputter-deposition because of their compatibility with CMOS (complementary metal–oxide semiconductor) process technology, and the characteristics of the fabricated thin film can be controlled by changing the sputtering conditions. Before the deposition, the chamber was evacuated to 7×10^{-4}Pa and the electrode material was deposited at room temperature without heating the substrate to fabricate a mechanically stable amorphous thin film.

To optimize the sputtering conditions for the sputtered IrOx and TiN thin films, each parameter in the deposition process was set to high (H) or low (L). A total of 16 IrOx and 16 TiN samples were fabricated under different sputtering condition combinations. Table I shows the details of the conditions of sputtered IrOx and TiN.

The basic electrochemical characteristics were evaluated by CV to measure charge storage capacity (CSC) in a three-electrode cell. CV was performed by activation using a triangular wave and repetitive cycling at a scan rate of 50 mV/s in a potential range from −0.65 to 0.85 V for IrOx [2], −0.85 to 0.85 V for TiN [3], and −0.6 to 1.05 V for Pt without H_2 and O_2 evolution in 0.01 M PBS (phosphate buffered saline). The CSC of the sputtered thin film can be calculated by the integration of the CV curve [4]. The surface morphology inspection was performed by AFM.

Table I. Sputtering conditions and CSC results of sputtered thin film

(a) IrOx

CSC (IrOx) (mC/cm²)	O_2 ratio	Low (20%)		High (80%)	
RF Power	Pressure / Time	Low (0.35 Pa)	High (1 Pa)		Low (0.35 Pa)
Low (50 W)	Low (30 min)	5.9 (A)	42.9 (B)	47.4(C)	44 (D)
	High (60 min)	2.7 (H)	53.8 (G)	70.1 (F)	59.4 (E)
High (200 W)		2.8 (I)	5.5 (J)	239.4 (K)	175.6 (L)
	Low (30 min)	2.9 (P)	7.4 (O)	138.2 (N)	122.9 (M)

(b) TiN

CSC (TiN) (mC/cm²)	N_2 ratio	Low (20%)		High (80%)	
DC Power	Pressure / Time	Low (0.5 Pa)	High (5 Pa)		Low (0.5 Pa)
Low (100 W)	Low (15 min)	1.4 (A)	1.5 (B)	1.5 (C)	1.4 (C)
	High (60 min)	2.0 (H)	5.8 (G)	3.9 (F)	3.1 (E)
High (500 W)		43.0 (I)	25.0 (J)	20.2 (K)	5.0 (L)
	Low (15 min)	11.0 (P)	7.7 (O)	7.7 (M)	4.3 (N)

[a] Correspondence to: Jun Ohta. E-mail: ohta@ms.naist.jp

Graduate School of Materials Science, Nara Institute of Science and Technology, 8916-5, Takayama, Ikoma, Nara 630-0192, Japan

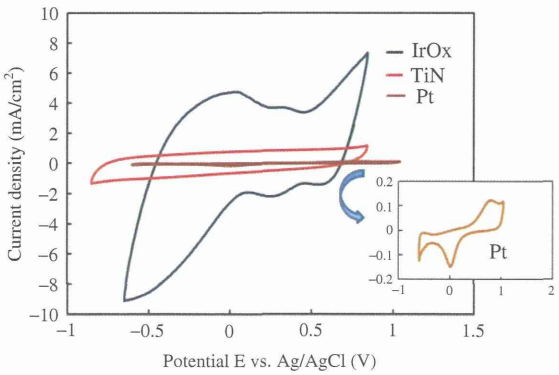

Fig. 1. CV curves of sputtered IrOx and TiN and compared with Pt

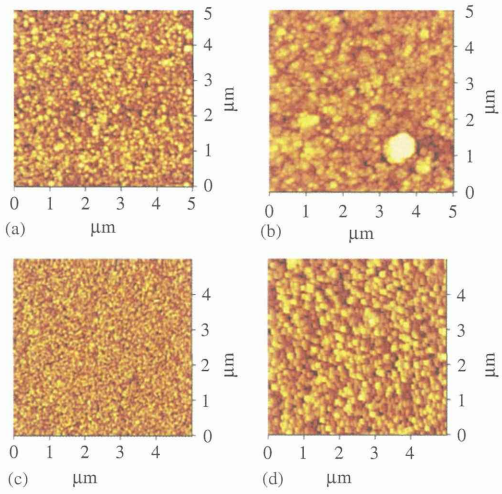

Fig. 2. AFM results of sputtered IrOx and TiN (a) IrOx (condition N), $R_a = 6.63$ nm; (b) IrOx (condition K), $R_a = 8.77$ nm; (c) TiN (condition F) $R_a = 8.21$ nm; and (d) TiN (condition K) $R_a = 10.55$ nm

In addition, to measure the CDC of IrOx and TiN, a balanced biphasic current pulse from 50 to 1200 μA, 60 Hz with a pulse width 0.5 ms was injected, the maximum voltage response of the input current pulse was measured without exceeding the range −0.6 to 0.8 V for IrOx and −0.8 to 0.8 V for TiN. The CDC of the electrode can be calculated from the maximum input balanced biphasic current pulse. Photoresist (SU-8, MicroChem Corp.) was coated on the sputtered thin film to a depth of 8 μm by lithography to form a 300-μm diameter electrode for measuring the CDC.

3. Results and Discussion

Figure 1 shows the CV curves of IrOx and TiN. The CV curve of Pt is included for comparison. The larger the enclosed area of the CV curve, the higher the CSC of the fabricated electrode. The CV curves show that IrOx has a better CSC than TiN. In addition, the CV curve of IrOx has distinct peaks, which shows that reduction–oxidation reactions are involved during the potential cycling. However, the CV curve of TiN has no distinct peaks, which indicates the electrode current is dominated by capacitive current flow [3]. The difference in the mechanisms of current injection is the reason why the CSC of IrOx is larger than that of TiN.

The CSC of the sputtered IrOx and TiN under different sputtering conditions calculated from the CV curve is also shown in Table I. It is apparent that the CSC of sputtered IrOx and TiN is related to the sputtering conditions. The CSC of IrOx shows a higher result than that of TiN. From the experimental results,

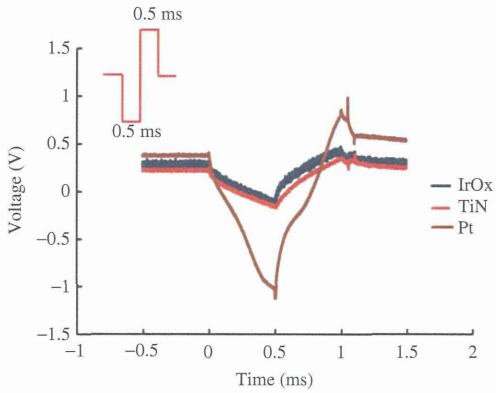

Fig. 3. Voltage response of balanced biphasic current pulse of IrOx under condition K and TiN under condition J and Pt

it can be seen that the O_2 partial pressure plays an important role in determining the CSC of IrOx. With the increase in O_2 partial pressure, the number of unbound iridium atoms Ir+x of the sputtered IrOx increases and they contribute to the charge transfer in the electrolyte [4]. Thickness is another factor that affects the CSC of the sputtered IrOx film, as can be seen from the experimental results. A thicker sputtered IrOx film probably has a larger CSC probably because a thicker IrOx film has a rougher surface, which increases the contact area between the electrode and the electrolyte, thus increasing the CSC of the electrode. However, sputtering pressure has no absolute effect on CSC. The CSC of TiN mainly depended on the sputtering time and power. Longer sputtering times and higher power lead to an increased thickness and a rougher surface. Figure 2 shows the AFM results of sputtered IrOx and TiN. The color range of the AFM image was expressed by 3 standard deviations. The roughness of the sputtered IrOx under condition N and K were 6.63, 8.77 nm and of TiN under condition F and K were 8.21 and 10.55 nm, respectively. The higher CSCs of the IrOx and TiN samples show that there was a larger roughness surface than in the case of low CSC samples. The rougher surface results in a larger surface area, leading to a larger CSC. Figure 3 shows the voltage response of the sputtered IrOx under condition K, sputtered TiN under condition J, and sputtered Pt, when the amplitude of the input biphasic current pulse was 300 μA. IrOx shows a smaller voltage in response to the biphasic current pulse than TiN and Pt. When the input biphasic current pulse equals 300 μA, the voltage response of IrOx and TiN is still within the safe voltage window; however, the Pt voltage is out of the safe voltage window of Pt and cannot be used. CDCs of the optimized IrOx and TiN were 0.7 and 0.43 mC/cm^2, respectively.

From the viewpoint of reducing the area of the electrode size and increasing the resolution of the electrically elicited image by retinal prosthesis, IrOx is a better choice than TiN. However, for long-term implantation, the durability and biocompatibility of IrOx and TiN need to be evaluated in future work.

4. Conclusion

This letter reported on the optimization and comparison of sputtered IrOx and TiN thin film electrodes for retinal prosthesis devices. From the CV curves, it could be seen that IrOx shows faradiac reaction; however, TiN showed capacitive reaction during cyclic potential. CDC showed much lower results than CSC because of the high frequency measurement in CDC; only part of the CSC has been used. Both CSC and CDC of IrOx showed superior performance than those of TiN. From the experimental results, it could be seen that the CDCs of IrOx and TiN under the best sputtering conditions improved by more than 7 and 4 times compared to that of Pt, respectively.

Acknowledgments

This work was supported by the Strategic Research Program for Brain Sciences from the Ministry of Education, Culture, Sports, Science and Technology of Japan.

References

(1) Ohta J, Tokuda T, Kagawa K, Furumiya T, Uehara A, Terazawa Y, Ozawa M, Fujikado T, Tano Y. Silicon LSI-based smart stimulators for retinal prosthesis. *IEEE Engineering in Medicine and Biology Magazine* 2006; **25**:47–59.

(2) Cogan S, Plante T, Mcintosh J. Sputtered iridium oxide films (SIROFs) for low-impedance neural stimulation and recording electrodes. *Proceedings of the IEEE Engineering in Medicine and Biology Society* 2004; **6**:4153–4156.

(3) Weiland J, Anderson D, Humayun M. In vitro electrical properties for iridium oxide versus titanium nitride stimulating electrodes. *IEEE Transactions on Biomedical Engineering* 2002; **49**:1574–1579.

(4) Wessling B, Mokwa W, Schnakenberg U. RF-sputtering of iridium oxide to be used as stimulation material in functional medical implants. *Journal of Micromechanics and Microengineering* 2006; **16**:S142–S148.